

# An Amyloid-Like C-Terminal Domain of Thrombospondin-1 Displays CD47 Agonist Activity Requiring Both VVM Motifs<sup>†</sup>

J. F. McDonald, J. M. Dimitry, and W. A. Frazier\*

Department of Biochemistry and Molecular Biophysics, Washington University School of Medicine, Box 8231, 660 South Euclid Avenue, St. Louis, Missouri 63110

Received January 27, 2003; Revised Manuscript Received July 10, 2003

**ABSTRACT:** Two VVM-containing peptides in the C-terminal domain (CBD) of thrombospondin-1 function as CD47 agonists. A recombinant form of the CBD (rCBD) has been expressed that contains both VVM sites and exhibits CD47-dependent binding of C32 melanoma cells when coated at concentrations 100× lower than the peptide 4N1K (kRFYVVMWkK). Circular dichroism and thioflavin T binding of a recombinant form of the C-terminal domain (rCBD) of thrombospondin-1 indicated a species highly enriched in  $\beta$ -sheet secondary structure, with spectra similar to those of amyloid proteins. Reduction of the CD signal with progressively higher concentrations of guanidine hydrochloride was correlated with a loss of cell-binding activity. Melanoma cell spreading on vitronectin was strongly stimulated by immobilized rCBD co-coated at concentrations more than 50× lower than 4N1K, and the effect was blocked by treatment with pertussis toxin, consistent with the known mediation of CD47 signaling by trimeric G<sub>i</sub>. Mutations of either or both VV sequences of rCBD (1037–38 and 1123–24 of TSP1) to GG had a modest effect on cell binding, a component of which was inhibited by heparin. However, all three mutants dramatically reduced the signaling-dependent stimulation of cell spreading, indicating that the VVM motifs of rCBD are structurally linked in CD47 activation.

The C-terminal domain of thrombospondin-1 (TSP1) (residues 964–1170 of human TSP1 referred to as the CBD) has been identified as the site of its interaction with CD47, or integrin-associated protein (IAP) (1–4). Through CD47, TSP1 and the CBD-derived peptide 4N1K can augment integrin-dependent processes in a number of cell types (5–9). The 4N1K sequence is derived from the first of two homologous regions containing VVM motifs, termed 4N1 and 7N1, in peptide mapping studies of cell adhesion to TSP1 (1, 10). 4N1K can stimulate spreading of platelets and C32 melanoma cells on sparse substrata, which are mediated by  $\alpha$ IIb $\beta$ 3 and  $\alpha$ v $\beta$ 3 integrin, respectively. 4N1K also stimulates the migration of endothelial cells and vascular smooth muscle cells, processes mediated by  $\alpha$ v $\beta$ 3 and  $\alpha$ 2 $\beta$ 1 integrin (9, 11). In SMC and platelets, 4N1K causes a rapid decrease in cAMP levels. In each of these systems, integrin activation by CD47 agonists is blocked by pretreatment of cells with pertussis toxin, which inactivates heterotrimeric G proteins of the G<sub>i</sub> family. These observations have led to the recent demonstration of a cholesterol-dependent receptor complex in which CD47, integrin, and heterotrimeric G<sub>i</sub> protein are components (11–13). Together, these data indicate that a CD47-dependent pathway can modulate signaling that results in higher affinity/avidity states of integrins.

The nature of the interaction of thrombospondin with the CD47-integrin-G protein complex remains unclear. Thrombospondin is a modular protein with globular domains at each

terminus connected by a stalk region comprised of type I, II, and III repeats, the last of which represents a series of Ca<sup>2+</sup>-binding loops (14–16). An RGD motif included in the last type III repeat can be a ligand for  $\beta$ 3 integrins under some conditions (14, 17). The proximity of the RGD sequence to the CBD has suggested a model in which both  $\beta$ 3 integrin and CD47 are simultaneously engaged by TSP1 (2). In addition to 4N1K, a second, more C-terminal region in the CBD, peptide 7N3, contains a VVM motif homologous to 4N1K suggesting that both sequences may be important for efficient interaction with CD47 (1, 3, 4, 10). The lack of activity shown for either peptide in which conservative VV to GG changes are made has been an important demonstration of specificity (6, 7, 9).

Recently, it has become possible to use CD47 null cells to test the specificity of the VVM peptides. These include aortic smooth muscle cells (SMC), fibroblasts and platelets derived from the CD47 null mice (11, 18, 19), a mutant line of human Jurkat leukemic cells lacking CD47 (20), and a CD47 null subclone of human ovarian carcinoma cells called OV10 (21). We have reported that CD47 null SMC cannot chemotax to 4N1K, and the peptide does not augment their  $\alpha$ 2 $\beta$ 1-dependent migration toward soluble collagen. Also, CD47 null mouse platelets fail to spread and aggregate on a fibrinogen-coated surface in response to 4N1K. However, Tulasne et al. (22) report that CD47-null platelets can be stimulated to aggregate by 4N1K but not 4NGG. Furthermore, Barazi et al. have recently reported that VVM peptides, but not GGM controls, stimulated  $\alpha$ 4 $\beta$ 1-dependent adhesion of CD47 null Jurkat T cells (23). Interestingly, this effect of VVM peptide in the CD47-null Jurkats was blocked by

<sup>†</sup> This work was supported by NIH Grants CA65872 and HL54390 (W.A.F.) and an NIH Fellowship F32-HL10209 (J.F.M.).

\* Corresponding author. Phone: (314) 362-3348. Fax: (314) 362-7183. E-mail: Frazier@biochem.wustl.edu.

pertussis toxin, indicating that the stimulatory effect was still  $G_i$  dependent, suggesting either another receptor for the peptides or a receptor-independent mode of action. This latter concern is heightened by the amphiphilic nature of both 4N1K and 7N3 peptides that have clusters of positive charge flanking a central hydrophobic region. All of these considerations have spurred efforts to express the CBD in active form and assess the activity of the two VVM motifs in the context of the domain.

We report here the expression and characterization of a recombinant C-terminal domain of TSP-1 (rCBD) that binds melanoma cells with high affinity and promotes their  $G_i$ -dependent spreading on vitronectin substrata. Mutations in either of the VVM sites homologous to the CD47-interacting peptides 4N1K or 7N3 reduce the ability of the rCBD to augment integrin function. Circular dichroism and thioflavin T spectra indicate that rCBD is highly enriched in  $\beta$ -sheet secondary structure and that the CD47-interacting sequences are most active when presented in this structural context.

## MATERIALS AND METHODS

**Materials.** Human vitronectin was obtained from Collaborative Biomedical Products (Bedford, MA). Generation of the mouse monoclonal anti-CD47 antibody, B6H12, has been previously described (24). Human TSP was purified as previously described from outdated platelets obtained from the Red Cross (25). The peptides used in this study were synthesized by the Protein and Nucleic Acid Chemistry Laboratory of Washington University School of Medicine as previously described (1). Ultrapure guanidine hydrochloride was from Gibco BRL. All other reagents were obtained from Sigma Chemical Co. (St. Louis, MO) unless otherwise specified.

**Protein Expression and Mutagenesis.** Protein expression of rCBD was carried out in the Lac I<sup>+</sup> *Escherichia coli* strain M15, using a pQE30 vector (Qiagen, Chatsworth, CA). The construct pQE30/CBD coded for an N-terminal hexa His tag linked to pro-964 of the thrombospondin-1 sequence by Gly-Ser and continued to Glu-1166 followed by Ser-Arg-Gly-Ala at the C-terminus (Figure 1A). The truncation was chosen to avoid mispairing of the single cysteine (corresponding to position 992 of native TSP-1) with a cysteine-rich region in the type III domain immediately upstream of the CBD and to isolate the expressed domain from the RGD motif, also contained within the upstream type III repeat. Bacteria were routinely grown in 1 L of LB medium supplemented with ampicillin and tetracycline and harvested following induction with IPTG in midlog phase. PCR-based site-directed mutagenesis of the pQE30/CBD construct was carried out using a Stratagene Quickchange kit, employing complementary primers containing the base changes required for VV to GG mutations. The primers used for mutagenesis of the 4N1 region were AGCCGCTTTTATGGTGGGATGTGGAAGCAA (5' to 3') and TTGCTTCCACATCCCACCATAAAA-GCGGCT (3' to 5') to obtain the C4GG construct. The primers used for mutagenesis of the 7N1 region were GGTTTCATTAGAGGGGGTATGTATGAAGGG (5' to 3') and CCCTTCATACATACCCCCTCTAATGAAACC (3' to 5') to obtain the C7GG construct. The quadruple mutant C47GG was obtained using the C4GG construct as the template for mutagenesis of the 7N1 region as before. All constructs were confirmed by sequence analysis.

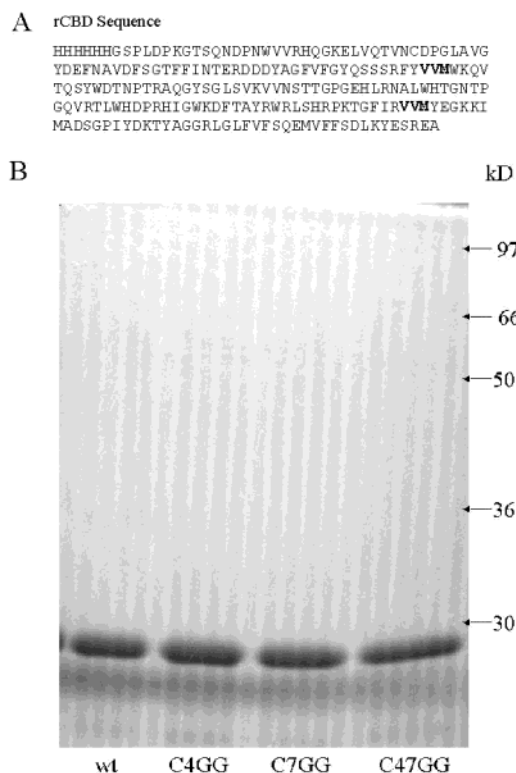


FIGURE 1: Recombinant rCBD and VVM mutants. (A) Sequence of recombinant C-terminal domain of thrombospondin-1 (rCBD). (B) Coomassie-stained 16% SDS-PAGE gel of rCBD and mutants carried out as described in Materials and Methods. From left to right: wt, C4GG, C7GG, and C47GG.

**Isolation and Characterization of rCBD.** *E. coli* expressing rCBD was suspended in 20 mM HEPES pH 7.5 containing protease inhibitors and lysed in a French press. Inclusion bodies were isolated and solubilized in 6 M guanidine-HCl and 50 mM phosphate pH 7.4, centrifuged to remove insolubles, and bound to Ni-NTA resin in the same buffer. The column was washed with 10 mM imidazole in 6 M guanidine-HCl and 50 mM phosphate pH 7.4, and the rCBD eluted with 50 mM imidazole in the same buffer. This preparation was loaded on an S-300 column equilibrated in 2 M guanidine-HCl, 20 mM HEPES pH 7, and 0.15 M NaCl and eluted between the void and the inclusion volumes. On the basis of the mobility of protein standards, it appeared that the rCBD eluted in an oligomeric form of higher order than a dimer (data not shown). The pooled fractions from several runs were utilized in that form, but solubility was also maintained by dialysis against 50 mM citrate pH 3, 0.15 M NaCl. The rCBD forms containing VV to GG mutations were isolated and treated in the same manner. SDS-PAGE analysis of each protein showed >90% purity of an approximately 30 kDa Coomassie-stained band (Figure 1B). Migration at the monomeric size was independent of the presence of reducing agents (data not shown). Thus, the protein, which contains a single free cysteine, did not dimerize. Furthermore, the presence of DTT or  $\beta$ -mercaptoethanol in the inclusion body solubilization buffer did not influence the S-300 column elution profile or the SDS-PAGE analysis. Solubility in the absence of guanidine was maintained at approximately 50  $\mu$ g/mL or less; however, it was convenient to prepare stock solutions in 2 M guanidine-HCl/HEPES and dilute coating solutions in the same buffer.

**Secondary Structure Prediction.** Analysis of primary sequence for secondary structure was performed using four separate Web-based programs through the ExpASy Molecular Biology Server of the Swiss Institute of Bioinformatics. These included PSIPRED, a modified Chou–Fasman method (26); PHDsec, which utilizes neural networks to make multiple sequence alignments (27); BMERC, which employs a nonglobular model more suitable for multimeric, multidomain, and transmembrane proteins (28); and JPRED, which determines a consensus from six methods by standardizing their input and output (29). The average  $Q_3$  score of these programs ranges from 73 to 78% based on the evaluation of extensive lists of known structures. Confidence values were standardized to a 1–9 (low to high) scale for this study based on probability calculations for the assigned structure of each residue.

**Cell Culture, Adhesion, and Spreading.** C32 human melanoma cells (ATCC CRL 1585) were cultured in Gibco Minimal Essential Medium (MEM) supplemented with 10% fetal bovine serum. Ovarian carcinoma cells that lack CD47 were stably transfected with  $\beta_3$  integrin and/or CD47(2) (20), cultured in Iscove's medium supplemented with 10% fetal bovine serum with appropriate antibiotic selection, and serum-starved before use in adhesion assays. Cell adhesion was performed in 96-well plates that were coated with substrates overnight at 4 °C. Plates were coated sequentially, with vitronectin at 37 °C for 2 h and then with the second substrate overnight at 4 °C. Each coating was followed by three washes with HEPES-buffered saline (HBS; 20 mM HEPES/NaOH, pH 7.4; 0.15 M NaCl). Immediately before assays were performed, wells were washed and blocked with 1% BSA in HBS. Cells were harvested with 0.4% EDTA in PBS and washed twice with PBS. For adhesion assays, cells were resuspended in HBS containing 0.4% BSA and allowed to adhere to the immobilized substrate for 30–60 min at 37 °C. After washing, the adherent cells were lysed in 1% Triton X-100 and quantified by endogenous phosphatase activity with *p*-nitrophenyl phosphate as a substrate (30). The cell number was adjusted so that maximal binding gave the highest absorbance within a linear range. For cell spreading assays, cells were resuspended in HBS containing 2 mM  $\text{CaCl}_2$ , 2 mM  $\text{MgCl}_2$ , and 0.4% HBS. Thirty min following addition to the wells, cells were washed, fixed, and stained with a Leukostat stain kit (Fisher Scientific, Pittsburgh, PA). Cell spreading was assessed by scoring cells in a microscopic grid. Spread cells were quantified by counting cells with a typical polygonal morphology and 50% or greater extranuclear cell area. The percentage of spread cells was calculated from the total cells in the grid, which ranged from 20 to 40. Duplicate fields were scored from triplicate wells for each condition. For inhibition of cell attachment or spreading, cells were preincubated with antibody for 15 min at 4 °C before the assay. When comparing effects of rCBD variants coated on surfaces, results were verified with at least two different preparations of each species with no discernible differences.

**Circular Dichroism.** Circular dichroism measurements were performed at 25 °C using 0.1 cm path length cells in a Jasco J715 Spectropolarimeter. All spectra are reported in terms of molar ellipticity or  $[\theta]$  in  $\text{deg cm}^2 \text{dmol}^{-1}$ . Far UV spectra were generated from an average of 10 runs, with each acquired with a scan speed of 20 nm/min. Samples were

dialyzed overnight against respective buffers, passed through a 0.2  $\mu\text{m}$  filter, and analyzed for protein concentration before measurement. For rCBD variants, at least two different preparations were employed with no significant differences in their spectra.

**Fluorescence Measurements.** Spectra were obtained using a PTI fluorescence spectrophotometer of 2.0-mL solutions containing 1.4 mM thioflavin T with rCBD in 50 mM borate pH 3 buffer with or without guanidine-HCl. Excitation spectra were recorded from 250 to 470 nm for emission at 482 nm. Emission spectra were recorded from 455 to 550 nm upon excitation at 450 nm.

**Protein Analysis.** Protein purity was assessed by SDS–PAGE using 16% Tris-glycine gels followed by Coomassie staining. Western analysis was performed to confirm protein identity following transfer to nitrocellulose, blocking and incubation with a primary antibody, HRP-conjugated secondary antibody, and development with ECL reagent (Amersham-Pharmacia). The protein concentration was determined by BCA assay (Pierce) or Bradford analysis (Bio-Rad).

## RESULTS

**Secondary Structure Prediction for C-Terminal Domain of TSP-1.** Four methods of secondary structure prediction were applied to the C-terminal CBD domain of TSP1, beginning with pro-964 at the N-terminal end, 36 residues downstream of the RGD motif, and ending with the native TSP1 C-terminus. All four methods employed indicated a species highly enriched in  $\beta$ -sheet, with 13–17 predicted regions of  $\beta$ -strands and a single consensus  $\alpha$ -helix. (Figure 2A). Using the modified Chou–Fasman method PSIPRED (26), values of 38.2%  $\beta$ -sheet and 15.9%  $\alpha$ -helix were determined, showing only slightly greater enrichment of  $\beta$ -sheet as compared to previous estimates for the C-terminal domain using a similar algorithm (16). However, for PHD, BMERC, and JPRED, which employ multiple sequence alignments derived from neural networks, the predicted  $\beta$ -sheet/ $\alpha$ -helix percentages were 49.3:6.3, 39.9:6.6, and 41.1:1.9%, respectively, exhibiting a more severe enrichment in  $\beta$ -sheet secondary structure. The extreme  $\beta$ -sheet/ $\alpha$ -helix ratios predicted for the native CBD may indicate that it is composed of extensive antiparallel sheets cross-hatched against each other as in the  $\beta$ -barrel structures of lactoglobulin or retinol-binding protein (31, 32). While interactions between TSP domains may result in some helix formation that is not predicted in the analysis of isolated CBD, the finding that the highest confidence values for  $\beta$ -structure are in the two VVM regions (Figure 2B) supports the idea that CD47-interacting motifs are present in the context of a  $\beta$ -sheet in the native structure.

**rCBD Is Enriched in  $\beta$ -Secondary Structure.** Circular dichroism experiments were performed to examine the folded state of the rCBD and to identify its secondary structural characteristics. These studies were carried out in 2 M guanidine under neutral pH conditions to optimize solubility. In the far UV region, a strong signal with a negative peak at 216 nm was observed for rCBD (Figure 3A), a pattern indicative of enrichment in  $\beta$ -sheet secondary structure. A similar CD spectrum was observed for rCBD solubilized in citrate buffer at pH 3 in the absence of guanidine (data not shown), indicating that guanidine treatment alone did not

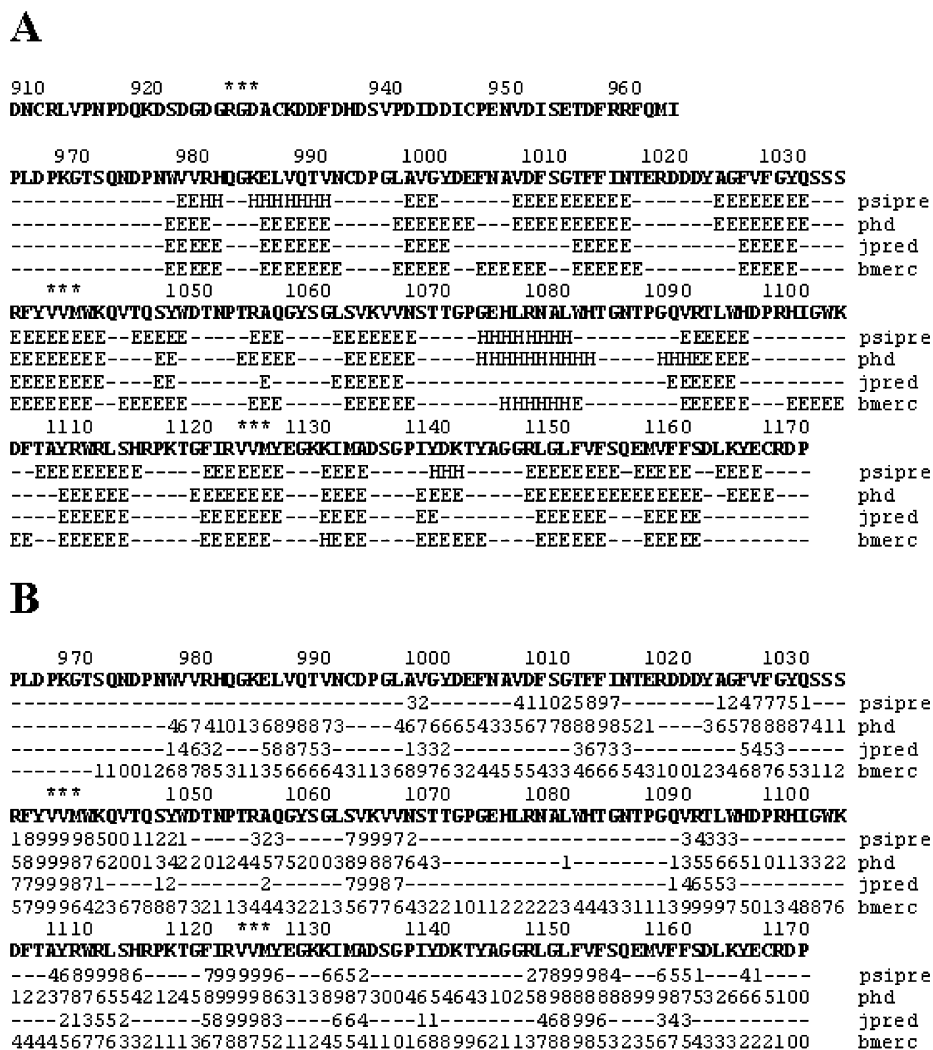


FIGURE 2: Analysis of sequence of thrombospondin-1 C-terminal domain. Primary amino acid sequence 908–1170 was obtained from the Swiss Protein Data Base under accession number P07996. Sequence numbers correspond to the residue under the last digit of each numeral. (A) Predicted secondary structures for CBD using four methods for each residue: H =  $\alpha$ -helix and E =  $\beta$ -sheet; all others are random coil, turn, or loop. Asterisks indicate RGD motif (at residue 926) and two VVM motifs (at residues 1037 and 1123). (B) Confidence values for  $\beta$ -sheet predictions for psipred, phd, and jpred on a 1–9 scale (lowest to highest). Values for bmerc are probabilities of the  $\beta$ -sheet for every residue on the same scale. (C) Sequence of rCBD.

confer a unique structure. The observed CD spectrum is distinct from proteins containing mixed  $\alpha$ -helix/ $\beta$ -sheet, which exhibit a more complex spectrum with negative peaks near 222 and 208 nm and a positive band below 200 nm (33). In fact, the absence of the positive band combined with a single negative band in the region of 216–218 nm is most indicative of amyloid formation. These structures, while classically observed with amyloid  $\beta$ -peptides and prion proteins (34–36), are also reported for amyloidogenic proteins such as transthyritin,  $\alpha$ -synuclein,  $\beta$ 2-microglobulin, and apolipoprotein C-II (37–40). For example, transthyritin and  $\alpha$ -synuclein exhibit peaks at 215 and 217 nm, respectively, following structural transitions with denaturants or high pH (37–39). Furthermore, the molar ellipticity minimum for the rCBD was within the range of that measured for other amyloids (i.e.,  $-10$  to  $-15$  deg  $\text{cm}^2 \text{dmol}^{-1}$ ) (37–40). It should be noted that guanidine-HCl per se does not induce amyloid structure, having often been used in denaturation studies of nonamyloidogenic proteins (41). These spectra and the limited solubility of the rCBD under neutral aqueous conditions are therefore indicative of amyloid-like

properties. A guanidine-HCl denaturation curve resulted in decreasing signal intensity at progressively higher guanidine concentrations but maintained approximately the same peak shape and minimum (Figure 3B). Thus, a  $\beta$ -sheet-rich structure was progressively denatured to a less ordered conformation.

To further explore the potential amyloid-like properties of the rCBD, thioflavin T (ThT) binding was employed. The fluorescence spectrum of this dye exhibits dramatic changes upon binding to amyloid and has been utilized as a quantitative indicator of its formation (42, 43). Transitions from mixed helix/sheet conformations to predominantly  $\beta$ -sheet in the presence of ThT produce a shift in the excitation maxima from below 350 nm to near 450 nm (37, 44) and in the emission peak from less than 450 nm to near 490 nm. Addition of rCBD to ThT resulted in a more than 6-fold increase in intensity of an excitation peak just below 450 nm (Figure 4A), and a similar increase in the emission peak near 490 nm (Figure 4B). The amplitude of the ThT maxima is comparable to results reported for other amyloidogenic proteins, including transthyritin and apolipoprotein

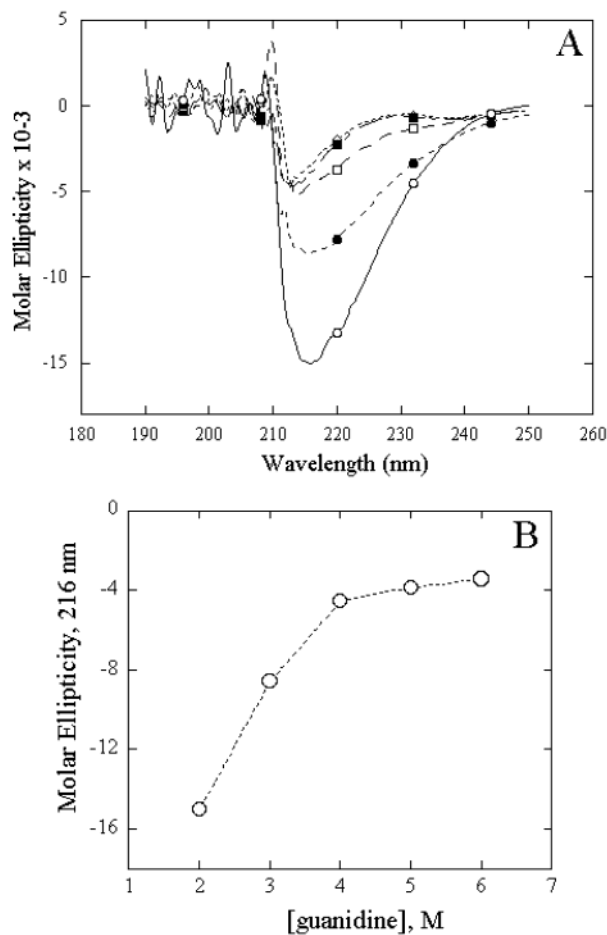


FIGURE 3: Detection of  $\beta$ -sheet structure in rCBD by circular dichroism. (A) CD spectra of rCBD ( $1 \mu\text{M}$ ) at increasing guanidine concentrations. (B) Guanidine denaturation curve taken from the 216 nm values from each spectra.

C-II. In addition, the binding of ThT to bovine serum albumin at the same concentration resulted in an increase of only about 50% over background, or a 12-fold lower signal than rCBD (data not shown). In buffer containing 2 M guanidine, the ThT fluorescence signal was linear with increasing protein (Figure 4C), an indication of tight and specific binding to  $\beta$ -sheet-enriched protein. Thus, rCBD is highly enriched in  $\beta$ -sheet and may share structural properties with amyloid proteins. Interestingly, treatment of  $5 \mu\text{M}$  platelet thrombospondin with ThT produced no specific binding (data not shown), suggesting that CBD in the context of the full-length native molecule is subject to intramolecular interactions that can shield it from oligomerization leading to amyloid formation.

Both the 4N1K and the 7N3 VVM-containing motifs (Figure 2A) have been identified as regions that can interact with CD47 (1, 10). However, the functional importance of these motifs in a larger structural context and the relationship between them in a model of CD47 activation has not been addressed. We therefore mutated the two VV dipeptide sequences to GG individually and together. The three resulting constructs are termed C4GG, C7GG, and C47GG for the two double mutants in each region and the quadruple mutant in both regions, respectively (Figure 1A). Circular dichroism analysis of the three mutants indicated that they possess the same  $\beta$ -sheet-rich structure as the wild type, with negative peaks at 215–216 nm (Figure 5). Furthermore, the

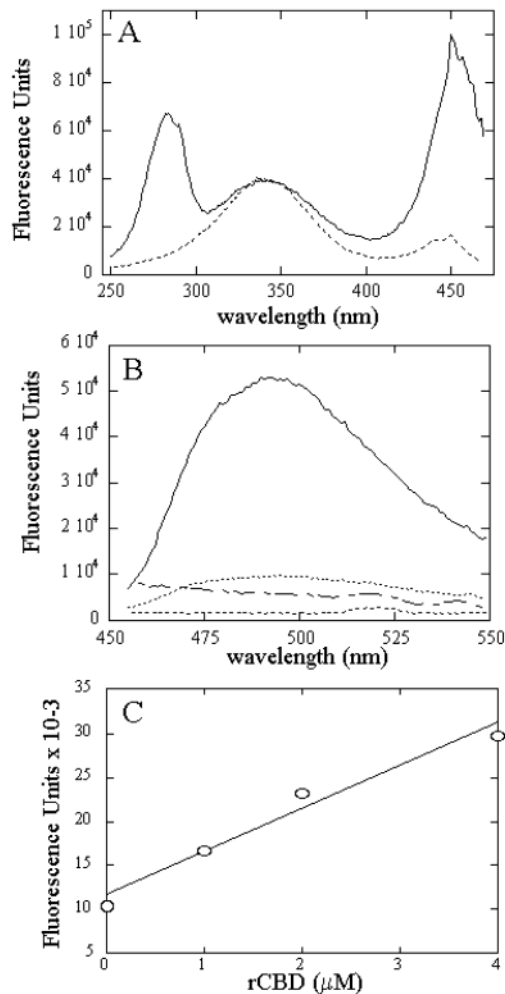


FIGURE 4: Detection of  $\beta$ -sheet structure in rCBD by Thioflavin T. (A) Excitation spectrum of  $1.7 \mu\text{M}$  ThT alone (dotted) and with  $1 \mu\text{M}$  rCBD (solid). (B) Emission spectra of buffer alone (dotted), ThT alone (small dots), rCBD alone (dotdash), and ThT with rCBD (solid). (C) Plot of ThT emission in 2 M guanidine with rCBD at indicated concentrations.

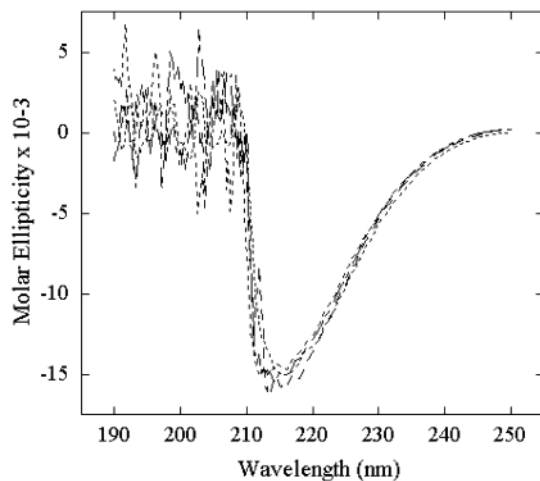


FIGURE 5: Circular dichroism of rCBD mutants with VV to GG changes. Wild type, solid; C4GG, dashed; C7GG, dotted; and C47GG, dotdash.

signal intensities in that region are within 10% of each other for all three constructs, indicating that the concentration of folded species in each preparation was similar. Thus, the VV

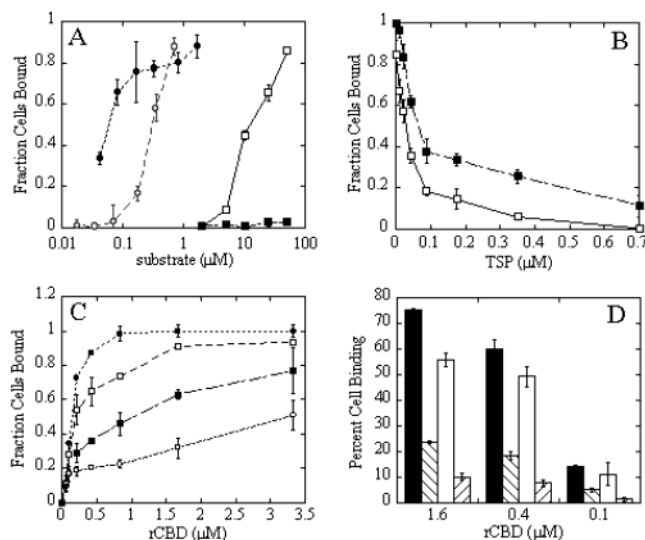


FIGURE 6: Cell attachment to rCBD substrata. (A) Comparison of C32 melanoma cell attachment to immobilized substrates on a molar basis. Plastic wells were coated with 4N1K (open squares), 4NGG (closed squares), CBD (closed circles), and TSP (open circles). Cell attachment was measured by the PNPP reaction following lysis. (B) TSP competition binding of C32 melanoma cells. Wells were coated with 1  $\mu\text{M}$  rCBD, and cells were treated with soluble TSP in HBS containing 0.4% BSA and either 2 mM  $\text{CaCl}_2$  (open circles) or 1 mM EDTA (closed circles) before attachment. (C) Effect of guanidine denaturation on C32 melanoma cell adhesion. Wells were coated with rCBD at indicated concentrations in HBS containing guanidine-HCl at 2 M (closed circles), 3 M (open squares), 4 M (closed squares), and 6 M (open circles). (D) Ovarian carcinoma cell attachment to rCBD. CD47+, black; CD47-, right-hatched; CD47+ with 1  $\mu\text{g}/\text{mL}$  heparin, white; and CD47- with 1  $\mu\text{g}/\text{mL}$  heparin, left-hatched. Error bars indicate standard deviation ( $n = 3$ ).

to GG changes had no impact on the overall secondary structure as determined by circular dichroism.

**CD47-Specific Cell Adhesion to rCBD Substrata.** Adhesion to immobilized substrates has been previously employed to identify CD47-binding sequences, using peptides derived from the CBD as well as TSP1 fragments containing the domain itself (1, 5, 7, 8, 10, 15, 45). It is also well-established that a substratum of full-length TSP1 can bind a number of cell types as well as stimulate spreading and induce effects on cell morphology (14, 17, 46–49). Furthermore, reports differ on whether melanoma cell binding by TSP1 requires the RGD sequence. These studies have employed fusion proteins for expression of the C-terminal domain that may interfere with CD47-interacting sites through misfolding or occlusion (3, 5, 45). In this study, rCBD with a minimal N-terminal appendage bound C32 melanoma cells when coated at molar concentrations approximately 100 $\times$  lower than 4N1K, the peptide derived from it (Figure 6A). The rCBD was nearly 10 $\times$  more potent on a molar basis than whole TSP1, perhaps indicating a steric hindrance by other regions of the TSP1 molecule. Soluble platelet TSP1 effectively inhibited binding, both in the presence and in the absence of calcium (Figure 6B). In calcium-containing buffer, the presence of soluble TSP1 resulted in nearly 90% inhibition of cell attachment at 350 nM and 50% at approximately 35 nM. In EDTA, the concentration of TSP1 required for 50% inhibition was slightly greater, indicating that unfolding of the calcium-binding domain had no direct effect on the availability of CD47-interacting sequences of

TSP1 to compete for binding with immobilized rCBD. Coating wells with rCBD in higher concentrations of guanidine resulted in progressively lower levels of binding (Figure 6C), although protein analysis showed that equivalent amounts were coated under these conditions (data not shown). As shown in Figure 3B, CD spectra of rCBD under similar conditions showed a progressive decrease in molar ellipticity; thus, the reduction in cell adhesion to rCBD can be correlated with the loss of  $\beta$ -sheet structure detected by circular dichroism. Coating the rCBD from acidic buffer, or from guanidine stock solutions directly into neutral aqueous buffer, also resulted in high affinity binding of melanoma cells (data not shown). Thus, an active conformation of rCBD that is rich in  $\beta$ -structure existed in aqueous buffer without a requirement for denaturants. An ovarian carcinoma cell line, OV10, deficient in CD47 expression was also employed to verify CD47-specific interaction. Stable transfectants of OV10, expressing  $\alpha\text{v}\beta 3$  integrin with and without CD47, have been previously employed to demonstrate enhanced cell binding of vitronectin-coated beads with CD47 expression. At concentrations of rCBD that support high levels of binding of CD47-expressing cells, the binding of cells deficient in CD47 was reduced to about 20% (Figure 6D). It was previously shown that CD47-mediated cell adhesion can be partially inhibited by heparin. With heparin treatment of the OV10 cells, an even greater dependence on CD47-mediated cell binding was observed (Figure 6D). Thus, a component of cell binding to rCBD is derived from CD47-independent glycosylaminoglycan interactions. Heparin eliminates this component of binding and reveals the CD47-dependent adhesion. Thus, cell-binding epitopes with discrete secondary structure are detected in rCBD that bind CD47 with high affinity and are inhibited by TSP1.

**Cell Binding to VVM Mutants of rCBD Displays Increased Heparin Sensitivity.** The binding of cells to three concentrations of the wild type and mutant rCBDs was compared. Concentrations were chosen to give maximal binding to wild type rCBD, approximately half-maximal, and low binding, about 10% of maximal specific binding (above that seen with peptide 4NGG). It should be noted that the binding curve of cells to wild type rCBD is very steep, with the majority of the change occurring over just a 4-fold concentration range (Figure 6A). This is consistent with highly cooperative, multivalent binding with many cell contact sites. No decrease in melanoma cell binding was found for any of the mutant species relative to wild type at the highest coating concentration; however, a partial but significant decrease with all three mutants occurred at 0.1  $\mu\text{M}$  rCBD, the level of about half-maximal binding for wild type (Figure 7A, left panel). All four rCBD species, including wild type, displayed a high degree of heparin sensitivity with respect to melanoma cell binding, and binding to all three VVM mutants was reduced at the higher coating concentrations relative to wild type rCBD (Figure 7A, right panel). Note that the C4GG mutant was the most sensitive to heparin, indicating that this site is responsible for most of the binding interaction. Binding to rCBD by CD47-transfected OV10 cells showed a reduction for all three VVM mutants at intermediate coating concentrations, but, as with the melanoma cells (Figure 7A), none were distinguished from wild type rCBD at higher concentrations (Figure 7B, left panel). However, the binding of OV10 cells to all of the rCBD mutants (Figure 7B) was more heparin

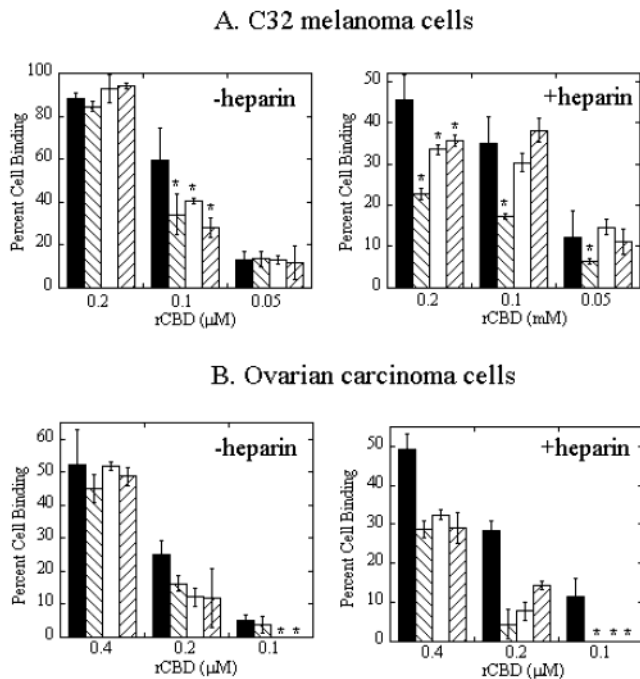


FIGURE 7: Effect of VV to GG changes on cell binding to rCBD. (A) C32 melanoma cell attachment to rCBD. Untreated cells, left panel; cells treated with 1  $\mu\text{g}/\text{mL}$  heparin, right panel. (B) Ovarian carcinoma cell attachment to rCBD. Cells stably transfected with  $\beta 3$  integrin and CD47 without treatment, left panel; cells treated with 1  $\mu\text{g}/\text{mL}$  heparin, right panel. Wild type, filled; C4GG, right-hatched; C7GG, open; and C47GG, left-hatched. Error bars indicate standard deviation ( $n = 3$ ). \* $p < 0.05$  relative to wt rCBD at each concentration.

sensitive than was the melanoma cell binding (Figure 7A). These results indicate that rCBD binds CD47 at the cell surface in the context of multivalent interactions that include heparin-inhibitable binding sites. Furthermore, the VVM sites of rCBD contribute a greater share of the cell-binding activity when heparin is used to swamp out interactions between cell surface glycans and the positively charged rCBD. Why the double mutant C47GG behaves like C7GG and not like C4GG is somewhat paradoxical (Figure 7A,B, right panels) and is not, at present, understood. However, altering the hydrophobic interactions surrounding the positive lysine and arginine residues may influence rCBD binding with cell surface glycans at the heparin-inhibited sites. This may occur through increased conformational flexibility because of the insertion of two Gly-Gly sequences in place of their Val-Val counterparts.

*C32 Cell Spreading on Vitronectin Substrata Is Stimulated by rCBD.* Melanoma cell spreading is an integrin-dependent phenomenon mediated by downstream signaling events emanating from  $\alpha v \beta 3$  activation upon binding of vitronectin (50). Through its association with both integrins and heterotrimeric  $G_i$ , CD47 provides a signaling link that modulates this process (2), as demonstrated by soluble 4N1K treatment of both melanoma cells on sparse vitronectin (7) and platelets on collagen (6). In this study, co-coating of rCBD with vitronectin strongly induced C32 cell spreading (Figure 8, top left and right; Figure 9A), as does 4N1K under the same conditions (Figure 8, middle left; Figure 9A), while 4NGG has no effect (Figure 8, middle right; Figure 9A). Treatment of cells with the function-blocking anti-CD47 antibody B6H12 reduced rCBD-stimulated spreading (Figure 8, bot-

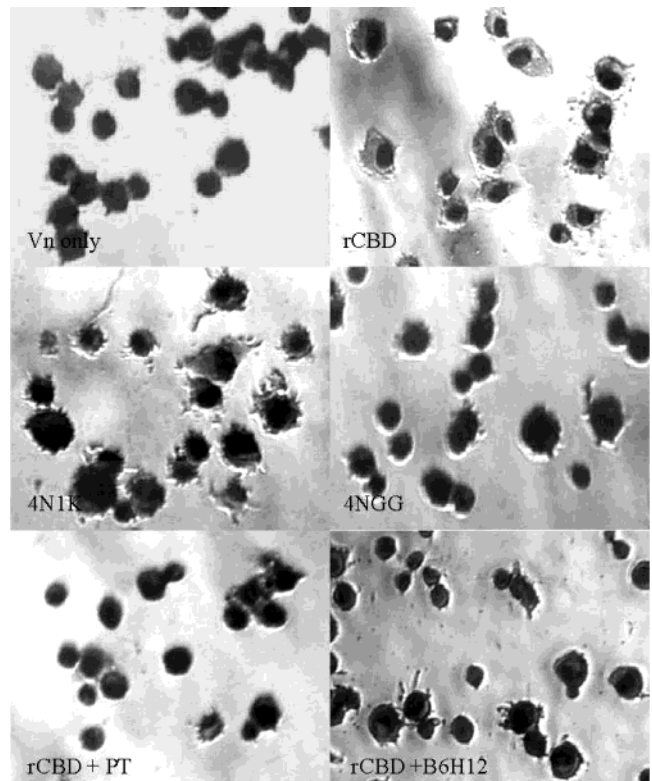


FIGURE 8: rCBD stimulates melanoma cell spreading on vitronectin. Microscopic images in a high-power field of cells spread on 1  $\mu\text{g}/\text{mL}$  vitronectin alone (upper left) or co-coated with 0.33  $\mu\text{M}$  rCBD (upper right), 20  $\mu\text{M}$  4N1K (middle left), or 20  $\mu\text{M}$  4NGG (middle right). C32 melanoma cells previously treated with 300 ng/mL pertussis toxin overnight (lower left) or with 100  $\mu\text{g}/\text{mL}$  B6H12 for 15 min (lower right) were placed on rCBD-vitronectin substratum and allowed to spread for 30 min. Cells were fixed and stained using the Leukostat kit.

tom right; Figure 9B), while treatment with a mIgG control did not (Figure 9B). Furthermore, overnight treatment of cells with pertussis toxin blocked rCBD-stimulated spreading (Figure 8, bottom left; Figure 9B), although binding to the rCBD-vitronectin substratum was unaltered (data not shown). These results are consistent with the modulation of integrins by heterotrimeric  $G_i$  and show that immobilized rCBD can activate CD47 in the same manner as 4N1K or whole TSP1. As with cell adhesion, the relative potency of rCBD to evoke this effect was 50–100 $\times$  greater than 4N1K on a molar basis. Previous studies have shown that 7N3, a peptide derived from the more C-terminal VVM motif in the CBD (Figure 2A), can stimulate cell spreading in the same manner (5). Thus, rCBD may combine the effects of both peptides, or a single site on CD47 may recognize either sequence. In either case, the difference in potency indicates that CD47 binding sites in the context of the rCBD molecule possess additional interactions that may increase its efficacy as an agonist for CD47.

*rCBD Mutants Are Defective in Signaling Cell Spreading.* To determine the effect of VV to GG mutations on signaling via stimulation of  $G_i$ -mediated CD47 actions, cell spreading was measured on sparsely coated vitronectin (1.0  $\mu\text{g}/\text{mL}$  coating concentration) co-coated with each mutant rCBD. As compared with wild type rCBD-stimulated spreading carried out in the same experiment, the activity of all three of the VV to GG variants was significantly reduced (Figure 10A). Even at coating concentrations resulting in maximal

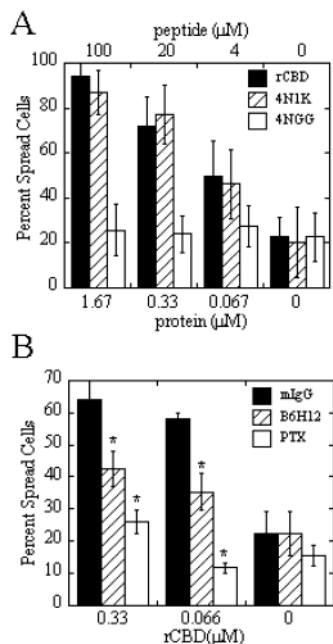


FIGURE 9: Relative activity and inhibition of cell spreading. (A) Comparison with peptides. Wells were co-coated with 1  $\mu\text{g}/\text{mL}$  vitronectin and rCBD (filled), 4N1K (hatched), or 4NGG (open) at the concentrations indicated on the upper and lower X-axes. Following a 30-min incubation at 37  $^{\circ}\text{C}$ , cells were treated and scored as described in Materials and Methods. (B) Inhibition of rCBD stimulation. Cells were spread on rCBD-vitronectin substratum after treatment with mIgG (filled) or B6H12 (hatched) at 100  $\mu\text{g}/\text{mL}$  for 15 min at 37  $^{\circ}\text{C}$  before spreading. Cells treated overnight with pertussis toxin before spreading (open). Error bars indicate standard deviation ( $n = 6$ ). \* $p < 0.05$  relative to control at each concentration.

binding of cells to each mutant (1  $\mu\text{M}$ , see Figure 6), at least a 50% reduction in spreading was observed. The effect was much more dramatic at lower concentrations of rCBDs (Figure 10B). At a 40 nM coating concentration, the wild type rCBD still supported nearly 70% of maximal spreading, while each of the mutants was completely inactive, and its stimulation was greater than any of the mutants coated at concentrations 25 $\times$  higher (Figure 10B). Differences among the three mutants were not great (Figure 10B) but seemed to parallel the small differences observed in cell binding (Figure 9A) (i.e., the C4GG species was somewhat less potent at a 200 nM concentration than either the C7GG or the C47GG variants, perhaps indicating a structural linkage between the two sites).

Thus, in summary, the effect of the VV to GG mutations in rCBD is most dramatically expressed in stimulation of cell spreading, as compared with more subtle effects on CD47-mediated cell binding that are only fully manifested upon heparin inhibition of the glycan-mediated binding. This indicates that although additional sites on the CBD, including those that interact with cell surface glycans, may influence its cell-binding activity, G<sub>i</sub>-dependent signaling resulting in stimulation of cell spreading is mediated by CD47 interactions with both VVM motifs in the CBD.

## DISCUSSION

In previous studies, recombinant forms of the CBD have been expressed either as species attached to other domains of the TSP1 molecule (8, 51) or as fusion proteins to facilitate

purification (3, 5, 45). The first approach limits the ability to observe strictly CD47-dependent effects since the other adjacent regions of TSP1 contain binding sites for integrins (12, 14, 17, 52, 53) and may form non-native complexes with the CBD because of disruption of normal interdomain interactions that are likely to be calcium dependent (15, 51). The fusion protein approach complicates structural analyses with the presence of non-native domains that themselves may interact with the CBD thus occluding or modifying receptor-binding sites. In this study, we report the isolation of an rCBD composed almost entirely of a native sequence that is highly enriched in  $\beta$ -sheet secondary structure and that promotes  $\alpha\text{v}\beta 3$ -dependent spreading of melanoma cells, a hallmark response of G<sub>i</sub>-coupled CD47 stimulation by TSP-derived agonists (7, 12, 13). Furthermore, we have shown that both VVM sequences are required for optimal CD47 activity, indicating a linkage between the sites for receptor activation. That rCBD binds and promotes spreading of C32 melanoma cells with a much greater potency than 4N1K indicates that there are structural determinants beyond the peptides themselves that allow for a more efficient or productive interaction. The degree of cell-binding activity preserved in all three mutants suggests that these features can overcome to some extent the disadvantageous, but conservative, VV to GG changes. However, the more serious defect in stimulation of cell spreading by the mutants indicates that the VVM motifs are critical for CD47 activation of G<sub>i</sub> signaling. The heparin-binding activity of rCBD may be a factor that compensates for differences in the CD47 affinity of the mutants to maintain cell binding, while not contributing to CD47 activation of G<sub>i</sub>.

The deficient activity of rCBD variants in either or both VVM sites suggests a binding mechanism featuring a bivalent interaction of CD47 with dual homologous sites, which would result in increased affinity derived from an additional binding contact. As mentioned previously, both 4N1K and 7N3 peptides can stimulate  $\alpha\text{v}\beta 3$ -dependent cell spreading. However, the 4N1K sequence is more highly conserved in all TSP isoforms as compared to the more degenerate 7N3 sequence, so the two sites may not be completely equivalent (1). Two general mechanisms can be postulated. One model would feature a single CD47 molecule with two binding sites, one for each VVM sequence. Binding at both VVM sites would initiate a conformational change that is transmitted to the cytoplasmic or transmembrane domains resulting in G protein coupling. Peptide agonists would presumably bind at both sites, but at a much lower affinity without a structural linkage. Alternatively, a single CBD may bind two CD47 molecules, one at each VVM site, thus inducing dimerization. This model is particularly attractive given that receptor dimerization or oligomerization is proposed for GPCR activation (54–56). A GPCR dimer also accommodates the distance and orientation requirements of residues that contact G protein subunits deduced from crystal structures (57). Peptide agonists such as 4N1K may induce conformational changes that promote dimerization, or they may act under conditions in which CD47 oligomers are already present, such as via association with integrins upon cell attachment to vitronectin. The VV to GG changes in rCBD mutants would lower the affinity of one site so that monomer binding is reduced (first model) or dimer formation is blocked (second model). The quadruple mutant may possess residual

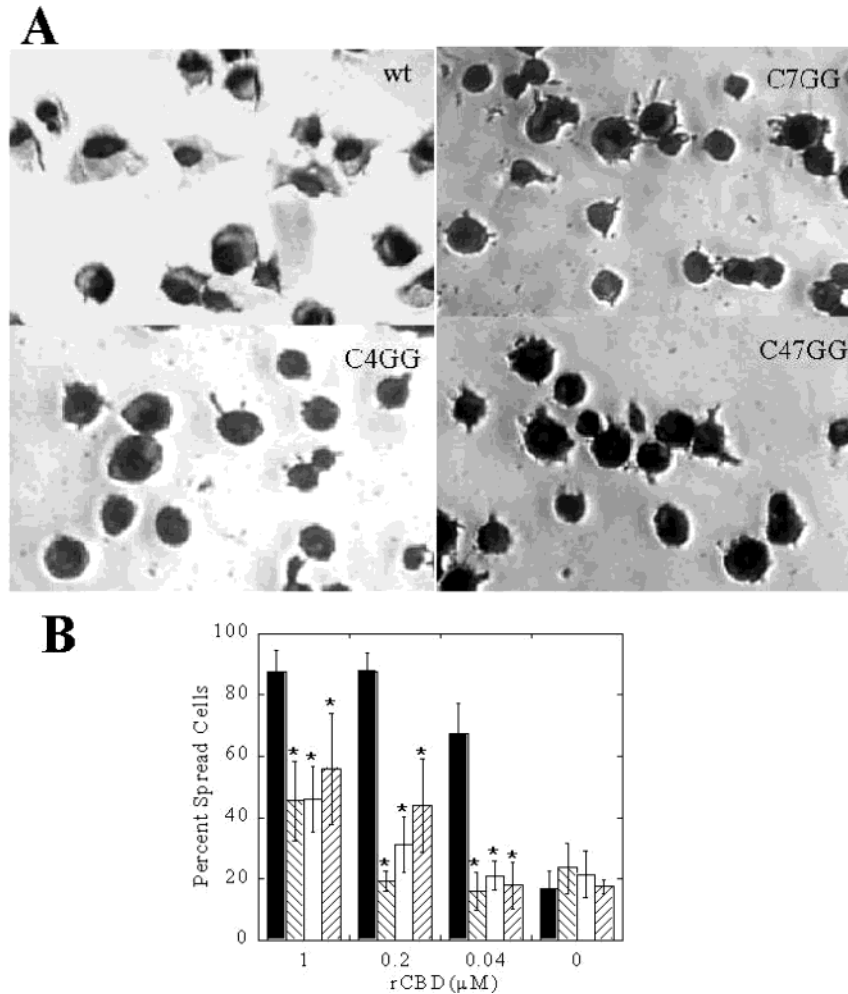


FIGURE 10: VV to GG mutants are deficient in stimulating cell spreading on rCBD-vitronectin substratum. (A) Microscopic images in a high-power field of cells spread on 1  $\mu\text{g}/\text{mL}$  vitronectin and 0.2 mM rCBD for 30 min at 37  $^{\circ}\text{C}$ . Cells were fixed and stained using the Leukostat kit. Wild type, upper left; C4GG, lower left; C7GG, upper right; and C47GG, lower right. (B) Plot of cell spreading on rCBD-vitronectin substratum under the same conditions. Spread cells were scored as described in Materials and Methods. Wild type, filled; C4GG, right-hatched; C7GG, open; and C47GG, left-hatched. Error bars indicate standard deviation ( $n = 6$ ). \* $p < 0.05$  relative to control at each concentration.

activity because some binding is maintained through other residues near the 4N1 and 7N3 sequences or from other structural determinants in the CBD. Decreased steric limitations upon substitution of glycines for valines may even allow compensatory movements of the rCBD chain that preserve a residual level of binding. The lack of activity of 4NGG peptide as a soluble agonist or as a coated substrate is an indication that other sites in rCBD interact with CD47 to promote binding or self-association.

The presence of an amyloid-like structure in the CBD determined by CD spectroscopy and ThT binding, along with the overwhelming indications from structure predictions in Figure 2, suggests that both VVM regions are incorporated in  $\beta$ -strands. These may interact or be in close proximity, despite a separation in primary sequence. Models of amyloid formation indicate that fibrils are formed from preamyloid intermediates that can contain native structure (29, 58, 59). Therefore,  $\beta$ -configurations in the CBD, as predicted by sequence analysis and confirmed by CD analysis here, may be preserved in stacked sheets and may even allow repeating motifs to be presented in close proximity to promote CD47 clustering at multiple sites on a fibril. The report that TSP1 is incorporated in Alzheimer's plaques in brain sections (60)

suggests that amyloid structure in rCBD represents a physiologically relevant form in addition to preserving a native structural element. A recent structural study of the C-terminal region of TSP-2, which reported a far UV-CD difference spectrum from recombinant fragments containing the proximal calcium-binding domain, also supported this conclusion (61). The general shape and minimum agreed quite well with the spectra we report, suggesting that both types of recombinant species represent highly enriched  $\beta$ -containing, natively-like structures. Interaction with the calcium-binding region apparently stabilized this structure and so may also influence CD47-binding epitopes in the CBD. In addition, an irreversible thermal transition associated with the CBD was reported in that study, which could represent CBD oligomerization (61). The structure of TSP1 exhibits a complex and potentially variable disulfide network, and many proteolytic cleavage sites have been documented, particularly in the type III regions proximal to the CBD (14, 68). Thus, the CBD may exist in a variety of truncated and folded forms, some of which may form amyloid-like structures. These combined observations make it likely that the CBD of native TSP is a  $\beta$ -enriched, preamyloid species whose CD47-binding epitopes are preserved with amyloid formation.

Furthermore, another study reports that a signaling complex containing CD47 mediates binding of microglia to amyloid peptides (62). The A $\beta$  peptides stimulate tyrosine phosphorylation of cellular proteins, which is modulated by 4N1K. Since amyloid peptides and fibrils are known to induce apoptosis in neuronal cells (63) and pancreatic islet cells (64), an intriguing possibility is that activation of these pathways are mediated by CD47-CBD interaction. Consistent with this hypothesis, anti-CD47 antibodies have been shown to induce apoptosis in Jurkat T-cells (65–67), and we have shown in recent experiments that rCBD and 4N1K promote apoptosis in smooth muscle cells (manuscript in preparation). The effect of heparin to inhibit cell binding of rCBD reported in this study (Figure 7) is consistent with this model since heparin is known to be associated with the amyloid (69) and can influence its deposition both positively and negatively (69, 70).

Another potentially relevant aspect of the amyloid-like structure of rCBD is the fact that mutations just upstream of the CBD in the calcium-binding domain of TSP5 or cartilage oligomeric matrix protein (COMP) are responsible for the spectrum of human genetic diseases called pseudoachondroplasia (PSACH) and multiple epiphyseal dysplasia (EDM1). In both diseases, mutant TSP5 molecules are expressed in chondrocytes and form electron dense deposits or precipitates within the secretory pathway that include other normally secreted matrix proteins as well (71, 72). Some of the earliest structural studies of TSP1 with electron microscopy indicated that the calcium-binding domain and the CBD of TSP1 interact in a calcium-dependent way to form the large C-terminal globular domain of calcium replete TSP1 (14, 15). Thus, the mutant calcium-binding domains that cause the PSACH and EDM1 phenotypes may allow or promote the formation of an amyloid-like organization of the TSP5 CBDs that could serve as a nucleating structure for the accumulation of other matrix proteins and chaperones found to be associated with these deposits (71, 72).

This study demonstrates that, while the binding interactions between the CBD and the CD47 may be complex, the two VVM sites, as originally defined by peptide studies (1), are indeed responsible for the stimulation of G<sub>i</sub>-dependent signaling by CD47. The ca. 100-fold increase in potency of the rCBD over the most active peptide, 4N1K, clearly indicates that the structural context of the CBD provides a more favorable presentation of the sequence motifs. The contribution of glycans to the interaction of the CBD with CD47, recognized even in the peptide studies (1, 23), appears to be relatively nonspecific as compared to the peptide motifs. The unexpected finding that rCBD adopts an amyloid-like,  $\beta$ -rich conformation provides a rationale for the presence of TSP at sites of amyloidogenic disease. Overall, this study has revealed structural insights of the CD47-TSP interaction that will contribute to future models of CD47 activation and allow a more detailed understanding of this important signaling system.

#### ACKNOWLEDGMENT

The authors thank Dr. Carl Frieden for assistance with collection of CD spectra and the use of the instrument.

#### REFERENCES

- Kosfeld, M. D., and Frazier, W. A. (1993) *J. Biol. Chem.* 268, 8808–8814.
- Brown, E. J., and Frazier, W. A. (2001) *Trends Cell Biol.* 11, 130–135.
- Gao, A.-G., and Frazier, W. A. (1994) *J. Biol. Chem.* 269, 29650–29657.
- Gao, A.-G., Lindberg, F. P., Finn, M. B., Blystone, S. D., Brown, E. J., and Frazier, W. A. (1996) *J. Biol. Chem.* 271, 21–24.
- Sipes, J. M., Kruttsch, H. C., Lawler, J., and Roberts, D. D. (1999) *J. Biol. Chem.* 274, 22755–22762.
- Chung, J., Gao, A. G., and Frazier, W. A. (1997) *J. Biol. Chem.* 272, 14740–14746.
- Gao, A.-G., Lindbergh, F. P., Dimitry, J. M., Brown, E. J., and Frazier, W. A. (1996) *J. Cell Biol.* 135, 533–544.
- Li, Z., Calzada, M. J., Sipes, J. M., Cashel, J. A., Kruttsch, H. C., Annis, D. S., Mosher, D. F., and Roberts, D. D. (2002) *J. Cell Biol.* 157, 509–519.
- Wang, X.-Q., and Frazier, W. A. (1998) *Mol. Biol. Cell* 9, 865–874.
- Kosfeld, M. D., and Frazier, W. A. (1992) *J. Biol. Chem.* 267, 16230–16236.
- Wang, X.-Q., Lindberg, F. P., and Frazier, W. A. (1999) *J. Cell Biol.* 147, 389–399.
- Frazier, W. A., Gao, A.-G., Dimitry, J., Chung, J., Brown, E. J., Lindberg, F. P., and Linder, M. E. (1999) *J. Biol. Chem.* 274, 8554–8560.
- Green, J. M., Zheleznyak, A., Chung, J., Lindberg, F. P., Sarfati, M., Frazier, W. A., and Brown, E. J. (1999) *J. Cell Biol.* 146, 673–682.
- Adams, J., and Lawler, J. (1993) *Curr. Biol.* 3, 188–190.
- Frazier, W. A. (1991) *Curr. Opin. Cell Biol.* 3, 792–799.
- Lawler, J., and Hynes, R. O. (1987) *Semin. Thromb. Hemostasis* 13, 245–254.
- Lawler, J., Weinstein, R., and Hynes, R. O. (1988) *J. Cell Biol.* 107, 2351–2361.
- Chung, J., Wang, X. Q., Lindberg, F. P., and Frazier, W. A. (1999) *Blood* 94, 642–648.
- Oldenberg, P. A., Gresham, H. D., Chen, Y., Izui, S., and Lindberg, F. P. (2002) *Blood* 99, 3500–3504.
- Reinhold, M. I., Green, J. M., Lindberg, F. P., Ticchoni, M., and Brown, E. J. (1999) *Int. Immun.* 11, 707–717.
- Campbell, I. G., Freemont, P. S., Foulkes, W., and Trowsdale, J. (1992) *Cancer Res.* 52, 5416–5420.
- Tulasne, D., Judd, B. A., Johansen, M., Asazuma, N., Best, D., Brown, E. J., Kahn, M., Koretzky, G. A., and Watson, S. P. (2001) *Blood* 98, 3346–3352.
- Barazi, H. O., Li, Z., Cashel, J. A., Kruttsch, H. C., Annis, D. S., Mosher, D. F., and Roberts, D. D. (2002) *J. Biol. Chem.* 277, 42859–42866.
- Brown, E. J., Hooper, T. H., and Gresham, H. (1990) *J. Cell Biol.* 111, 2785–2794.
- Santoro, S. A., and Frazier, W. A. (1987) *Methods Enzymol.* 144, 438–446.
- Jones, D. T., Taylor, W. R., and Thornton, J. M. (1994) *Biochemistry* 33, 3038–3049.
- Rost, B., and Sander, C. (1993) *J. Mol. Biol.* 232, 584–599.
- Stultz, C. M., White, J. V., and Smith, T. F. (1994) *Math. Biosci.* 119, 35–75.
- Cuff, J. A., Calmp, M. E., Siddiqui, A. S., Finlay, M., and Barton, G. J. (1998) *Bioinformatics* 14, 892–893.
- Prater, C. A., Plotkin, D. J., and Frazier, W. A. (1991) *J. Cell Biol.* 112, 1031–1040.
- Papiz, M. Z. (1984) *Nature* 324, 383–385.
- Flower, D. R., North, A. C. T., and Sansom, C. E. (2000) *Biochim. Biophys. Acta* 1482, 9–24.
- Woody, R. W. (1995) *Methods Enzymol.* 246, 34–71.
- Rochet, J.-C., and Lansbury, P. T. (2000) *Curr. Opin. Struct. Biol.* 10, 60–68.
- Ashall, F., and Goate, A. M. (1994) *Trends Biol. Sci.* 19, 42–46.
- Rosenblum, W. I. (2002) *Neurobiol. Aging* 23, 231–235.
- Conway, K. A., Harper, J. D., and Lansbury, P. T. (2000) *Biochemistry* 39, 2552–2563.
- El-Agnaf, O. M. A., Jakes, R., Curran, M. D., Middleton, D., Ingenito, R., Bianchi, E., Pessi, A., Neill, D., and Wallace, A. (1998) *FEBS Lett.* 440, 71–75.

39. Goldsteins, G., Andersson, K., Olofsson, A., Dacklin, I., Edvinsson, A., Baranov, V. O. S., Thylen, C., Hammarstrom, S., and Lundgren, E. (1997) *Biochemistry* 36, 5346–5342.
40. McParland, V. J., Kad, N. M., Kalverda, A. P., Brown, A., Kirwin-Jones, P., Hunter, M. G., Sunde, M., and Radford, S. E. (2000) *Biochemistry* 39, 8735–8746.
41. Pace, C. N. (1986) *Methods Enzymol.* 131, 266–80.
42. Levine, H. (1995) *Amyloid* 2, 1–6.
43. LeVine, H. (1999) *Methods Enzymol.* 309, 274–284.
44. Hatters, D. M., MacPhee, C. E., Lawrence, L. J., Sawyer, W. H., and Howlett, G. J. (2000) *Biochemistry* 39, 8276–8283.
45. Kosfeld, M. D., Pavlopoulos, T. V., and Frazier, W. A. (1991) *J. Biol. Chem.* 266, 24257–24259.
46. Adams, J. C., Kureishy, N., and Taylor, A. (2001) *J. Cell Biol.* 152, 1169–1182.
47. Bornstein, P. (1995) *J. Cell Biol.* 130, 503–506.
48. Narouz-Ott, L., Maurer, P., Nitsche, D. P., Smyth, N., and Paulsson, M. (2000) *J. Biol. Chem.* 275, 37110–37117.
49. Sun, X., Skorstengaard, K., and Mosher, D. F. (1992) *J. Cell Biol.* 118, 693701.
50. Schvartz, I., Seger, D., and Shaltiel, S. (1999) *Int. J. Biochem. Cell Biol.* 31, 539–544.
51. Missenheimer, T. M., Hahr, A. J., Harms, A. C., Annis, D. S., and Mosher, D. F. (2001) *J. Biol. Chem.* 276, 45882–45887.
52. Brown, E. J. (2001) *J. Clin. Invest.* 107, 1499–1500.
53. Li, Z., Calzada, M. J., Sipes, J. M., Cashel, J. A., Krutsch, H. C., Annis, D. S., Mosher, D. F., and Roberts, D. D. (2002) *J. Cell Biol.* 157, 509–519.
54. Gouldson, P. R., Dean, M. K., Snell, C. R., Bywater, G., and Reynolds, C. A. (2001) *Protein Eng.* 14, 759–767.
55. Cvejic, S., and Devi, L. A. (1997) *J. Biol. Chem.* 272, 26959–26964.
56. Singer, A. N., Walso, G. C., Harden, T. K., and Sondek, J. (2002) *Nat. Struct. Biol.* 9, 32–36.
57. Rios, C. D., Jordan, B. A., and Devi, L. A. (2001) *Pharmacol. Therapeut.* 92, 71–87.
58. Rodriguez-Frenandez, J. L. (1999) *BioEssays* 21, 1069–1075.
59. Kelly, J. W. (1997) *Structure* 5, 595–600.
60. Buee, L., Hof, P. R., Roberts, D. D., Delacourte, A., Morrison, J. H., and Fillit, H. M. (1992) *J. Pathol.* 141, 783–788.
61. Misenerheimer, T. M., Hannah, B. A., Annis, D. A., and Mosher, D. F. (2003) *Biochemistry* 42, 5125–5132.
62. Bamberger, M. A., Harris, M. E., McDonald, D. R., Husemann, J., and Landreth, G. E. (2003) *J. Neurosci.* 23, 2665–2674.
63. LeBlanc, A., Liu, H., Goodyer, C., Bergeron, C., and Hammonds, J. (1999) *J. Biol. Chem.* 274, 23426–23436.
64. Saafi, E. L., Konarkowska, B., Zhang, S., Kistler, J., and Cooper, G. T. (2001) *Cell Biol. Int.* 25, 339–350.
65. Li, Z., He, L., Wilson, K. E., and Roberts, D. D. (2001) *J. Immunol.* 166, 2427–2436.
66. Peterson, R. D., Hestdal, K., Olafson, M. K., Lie, S. D., and Lindberg, F. (1999) *J. Immunol.* 162, 7031–7040.
67. Manna, P. P., and Frazier, W. A. (2003) *J. Immunol.* 170.
68. Dardik, R., and Lahav, J. (1987) *Eur. J. Biochem.* 168, 347–55.
69. McLaurin, J., Franklin, T., Kuhns, W. J., and Fraser, P. E. (1999) *Amyloid* 6, 233–243.
70. Sabo, S., Lambert, M. P., Kessey, K., Wade, W., Kraft, G., and Kline, W. L. (1995) *Neurosciences Lett.* 184, 25–28.
71. Cohlberg, J. A., Li, J., Uversky, V. N., and Fink, A. L. (2002) *Biochemistry* 41, 1502–1511.
72. Kleerekoper, Q., Hecht, J. T., and Putkey, J. A. (2002) *J. Biol. Chem.* 277, 10581–10589.

BI0341408